www.lajss.org
Latin American Journal of Solids and Structures 3 (2006) 161–174

Boundary integral simulations of three-dimensional inviscid flows

Ricardo Caiado Alvarenga and Francisco Ricardo Cunha*

University of Brasilia, Brasilia, Brazil

Abstract

In this article we describe a boundary integral method for calculating the incompressible potential flow around arbitrary, lifting, three-dimensional bodies. By using Green theorems to the inner and outer regions of the body and combining the resulting expressions we obtain a general integral representation of the flow. The body surface is divided into small quadrilateral and triangular elements and each element has a constant singularities distribution of sinks and dipoles. An internal constraint is used and the sink distribution is determined by an external Neumann boundary condition. The application of Kutta's condition is quite simple; no extra equation or trailing-edge velocity point extrapolation are required. The method is robust with a low computational cost even when it is extended to solve complex three-dimensional body geometries. Calculations of the pressure coefficient, lift coefficient and induced drag coefficient are computed by the boundary integral numerical simulations. The boundary integral code developed here is verified by comparing the numerical predictions with experimental measurements, analytical solutions and results of the lifting-line theory and vortex-lattice method.

Keywords: boundary integral method, potential flow, three-dimensional body, pressure coefficient

1 Introduction

The field of computational fluid dynamics has made much progress in recent years. Computational methods for three-dimensional flows have been extensively used to solve problems in aerodynamics. For many times a flow problem was solved using hydrodynamic potential theory and such method has been found to agree well with experiment over a large range of flow conditions. Even when potential results fail to give the proper experimental values, they are frequently useful in predicting the incremental effect of a proposed design change or in ordering various designs in terms of effectiveness [20]. This agreement with real flow, combined with their geometric generality and low computational cost, has made numerical potential flow methods a great design tools in several applications.

Boundary integral equation methods for solving potential flow problems became feasible with the advent of digital computers. The method of Hess [6–9] was developed at Douglas Aircraft

*Corresp. author Email: frcunha@unb.br Received 18 Jun 2005; Revised: 22 Oct 2005

Company to solve flows about arbitrary three-dimensional lifting bodies by using the Newman boundary condition. His method is based on constant source and quadratic dipole densities distributed in the panel surface. Rubbert and Saaris [22] developed a similar method,however instead of dipoles they use vortices in the camber line of the wing. The boundary integral method proposed by Morino [17, 18] applies Green theorem and the Huygen's principle to solve steady and oscillatory, subsonic and linearized supersonic flows around arbitrary three-dimensional bodies. His method applies potential constant in each grid element and an internal Dirichlet boundary condition with Newman boundary condition in order to determine the dipole and source intensities. Maskew [15, 16] developed a panel code called VSAERO. His code uses the method of Morino to solve steady and unsteady subsonic flows. Ashby [2, 3] under contract with NASA, developed the panel code PMARC. His code like VSAERO is a low order panel method and uses the method of Morino. The method developed by Tinoco *et al* [24] at Boeing Commercial Airplane Company uses high order surface singularities with continuity in the grid element edges. The user can specify Newman boundary condition, Dirichlet boundary condition or both. Woodward [25, 26] developed a method that uses surface and lines of singularities and solve subsonic and supersonic steady flows. Singh *et al* [23] developed a boundary integral that considers internal singularity distributions and Newman boundary condition. Morino and Lemma [12, 19] and Gebhardt *et al* [13] developed an iterative boundary integral method to solve the full potential equation for transonic flows. Romate [21] calculate the local truncation errors in the approximations made in the usual boundary integral methods called panel methods. Similar applications of the boundary integral method using hydrodynamic potential in Stokes flow has been explored by Cunha *et al.* [4]. The present work presents a boundary integral method in the same way of Morino's method in order to simulate steady subsonic flow around three-dimensional potential flow around arbitrary bodies. We have tested our boundary integral code by calculating the pressure coefficient for several body geometries and comparing these results with others theoretical results and experimental observations.

2 Governing equation

If the flow is considered to be irrotational, incompressible and inviscid then the governing equation of the flow is the well-known Laplace equation:

$$\nabla^2 \Phi = 0 \tag{1}$$

we decompose the harmonic potential as $\Phi = \varphi^D + \varphi^\infty$, where φ^∞ corresponds to the incident flow that prevails even in the absence of the body, and φ^D is the disturbance potential due to the body which decays to zero at large distance from the body. For an arbitrary body, we can specify the kinematics boundary condition

$$\boldsymbol{U}_N = \boldsymbol{n}_i \cdot \boldsymbol{\nabla \Phi} = 0 \tag{2}$$

here n_i is the unit vector normal to the body's surface and U_N is the component of the velocity normal to the impenetrable boundaries. In addition, the disturbance created by the body vanish at infinity, therefore

$$\lim_{r\to\infty} \boldsymbol{\nabla}\boldsymbol{\phi}^D = 0 \tag{3}$$

where r is the relative distance between two points in the fluid. Equations (1), (2) and (3) constitute the potential problem to be solved.

3 Integral representation of the flow

In this section we discuss a three-dimensional boundary integral method to solve Laplace equation in terms of singularities distributions on an arbitrary body surface. For this end, we first shall show how to recast a differential formulation in an integral representation of the flow with Green's function theory.

3.1 Green's functions of the three-dimensional Laplace equation

By definition, a three dimensional Green's function satisfies the singular forced Laplace equation

$$\nabla^2 G\left(\boldsymbol{x}, \boldsymbol{x}_0\right) + \delta\left(\boldsymbol{x} - \boldsymbol{x}_0\right) = 0 \tag{4}$$

where δ is the three-dimensional delta distribution, and $\boldsymbol{x}_0$ is the location of the Green's function, also called the pole. The free-space Green's function corresponds to an infinite domain of flow with no interior boundaries. Solving Eq. (4) by using the 3D pair of Fourier transforms, we found the Green's function in the wave space $\boldsymbol{k}$

$$G\left(\boldsymbol{k}\right) = -\frac{1}{\left(2\pi\right)^{3/2}} \frac{e^{-i\boldsymbol{k}\cdot\boldsymbol{x}_0}}{k^2} \tag{5}$$

Performing the inverse Fourier transform it gives [14]

$$G\left(\boldsymbol{x}, \boldsymbol{x}_0\right) = \frac{1}{4\pi r} \tag{6}$$

that corresponds to the fundamental solution of a potential flow in the free space.

3.2 Description of the flow problem

We start with the Green's second identity [11] that states:

$$\int_S \left(\varphi_1 \boldsymbol{\nabla}\boldsymbol{\phi}_2 - \varphi_2 \boldsymbol{\nabla}\boldsymbol{\phi}_1\right) \cdot \boldsymbol{n}_i dS = \int_V \left(\varphi_1 \nabla^2 \varphi_2 - \varphi_2 \nabla^2 \varphi_1\right) dV \tag{7}$$

and φ_1 and φ_2 are two scalar functions of position. V and S represents the volume and its boundary surface of an arbitrary region of the flow and $\mathbf{n}$ is the unit vector normal to the

surface S . Whether both φ_1 and φ_2 are harmonic the right hand side vanishes, yielding the reciprocal relation for harmonic functions

$$\int_S \varphi_1 \boldsymbol{\nabla}\boldsymbol{\phi}_2 \cdot \boldsymbol{n} dS = \int_S \varphi_2 \boldsymbol{\nabla}\boldsymbol{\phi}_1 \cdot \boldsymbol{n} dS \tag{8}$$

Now, let's consider an arbitrary body composed of a boundary S_B, a wake S_W and an outer boundary S_∞ at infinity as sketched in the Fig. 1. The unit vector $\boldsymbol{n}_i$ or $\boldsymbol{n}$ is defined always pointing outside the region of interest. So, $\boldsymbol{n}_i = -\boldsymbol{n}$.

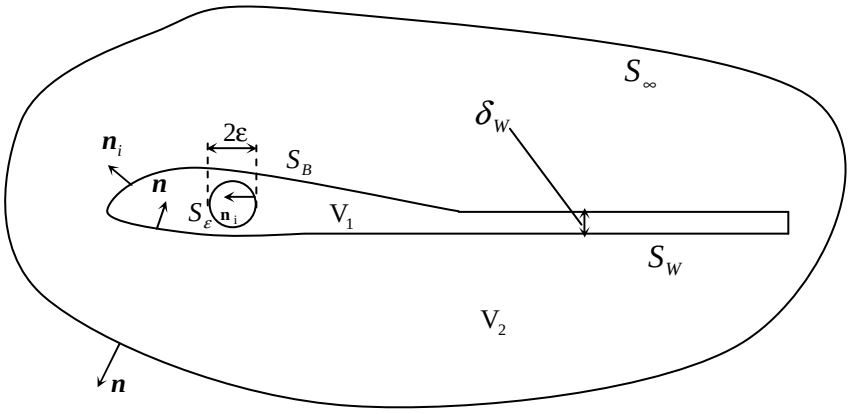

Figure 1: Sketch of an arbitrary body for the description of the 3D potential flow

In Eq. (8) the surface integral is taken over all the boundaries. Consider φ_1 as the fundamental solution $G = 1/4\pi r$, the unknown potential $\varphi_2 = \Phi_i$ and $S = S_B \cup S_W \cup S_\infty$. According to Fig. 1 Φ_i is the total potential in the domain V_1 (i.e. inside the body) and φ_1 is a potential of a sink and is singular as $r \to 0$. When exists a singularity located at $\boldsymbol{x}_0$ in the domain V_1, it is needed to be excluded from the region of integration. This singularity is bounded by a small sphere of radius ε. Outside of the small sphere, in the remaining domain V_1, the potential φ_1 satisfies Laplace equation . The potential φ_2 satisfies Laplace equation in all domain V_1. So the reciprocal relation, applied to the domain V_1 subtracting the volume of the singularity, yields

$$\int_{S_B, S_W, S_\varepsilon} (G(r)\boldsymbol{\nabla}\boldsymbol{\Phi}_i) \cdot \boldsymbol{n}_i dS - \int_{S_B, S_W, S_\varepsilon} (\Phi_i \boldsymbol{\nabla}\boldsymbol{G}(r)) \cdot \boldsymbol{n}_i dS = 0 \tag{9}$$

where the free space Green's functions corresponding to a point source and a potential dipole are given respectively by $G(r) = 1/4\pi r$; $\boldsymbol{\nabla}\mathrm{G}(r) = \boldsymbol{\nabla}\,(1/r)/4\pi = -\boldsymbol{r}/4\pi r^3$. Here, $\boldsymbol{r} = \boldsymbol{x} - \boldsymbol{x}_0$ with $\boldsymbol{x}$ being an arbitrary point of the flow and $\boldsymbol{x}_0$ the location of the singularity.

Considering the integral over S_ε containing the singularity, we write $dS = \varepsilon^2 d\Omega$, where $d\Omega$ is the differential solid angle, that is, the differential area of the sphere of unit radius, and using $G(r) = 1/4\pi\varepsilon$ and $\boldsymbol{\nabla}\mathrm{G}(r) = -\boldsymbol{n}_i/4\pi\varepsilon^2$ where the unit normal vector $\boldsymbol{n}_i = \boldsymbol{r}/\varepsilon$, we can write for

the limit as ε tends to zero that

$$\lim_{\varepsilon\to 0}\int_{S_\varepsilon} G(r)\boldsymbol{\nabla}\boldsymbol{\Phi}_i\cdot\boldsymbol{n}_i dS = \lim_{\varepsilon\to 0}\int_{S_\varepsilon}\frac{1}{4\pi\varepsilon}\boldsymbol{\nabla}\boldsymbol{\Phi}_i\cdot\boldsymbol{n}_i\varepsilon^2 d\Omega = O(\varepsilon)\to 0 \tag{10}$$

$$\lim_{\varepsilon\to 0}\int_{S_\varepsilon}\Phi_i\boldsymbol{\nabla}\boldsymbol{G}(r)\cdot\boldsymbol{n}_i dS = \lim_{\varepsilon\to 0} -\int_{S_\varepsilon}\Phi_i\frac{1}{4\pi\varepsilon^2}d\Omega\varepsilon^2 = -\Phi_i(\boldsymbol{x}_0) \tag{11}$$

Consequently, Eq. (9) reduces to

$$\Phi_i(\boldsymbol{x}_0) = \int_{S_B,S_W} G(r)\boldsymbol{\nabla}\boldsymbol{\Phi}_i\cdot\boldsymbol{n}dS - \int_{S_B,S_W}\Phi_i\boldsymbol{\nabla}\boldsymbol{G}(r)\cdot\boldsymbol{n}dS \tag{12}$$

The two integrals on the right-hand side represent a boundary distribution of the Green's function $G(r) = 1/4\pi r$ and of the Green's function $\boldsymbol{\nabla}\boldsymbol{G}(r) = (1/4\pi)\,\nabla\,(1/r)\cdot\boldsymbol{n}$ oriented perpendicular to the boundaries of the control volume, amounting to boundary distributions of points sinks and point dipoles. By analogy with corresponding results in the theory of electrostatics, concerning distributions of electric charges and charges dipole, we called the two integrals in Eq. (12) the single-layer and double-layer potential.

Now consider a situation when the flow of interest V_2 occurs outside the boundary of $S_B\cup S_W$ and the resulting total potential is Φ. For this flow the pole $\boldsymbol{x}_0$ (which is in the region V_1) is interior to $S_B\cup S_W$, and applying Eq. (8) it leads to:

$$\int_S G\boldsymbol{\nabla}\boldsymbol{\Phi}\cdot\boldsymbol{n}dS - \int_S\Phi\boldsymbol{\nabla}\boldsymbol{G}\cdot\boldsymbol{n}dS = 0 \tag{13}$$

A more appropriated equation can be obtained in terms of the jump condition $\Phi-\Phi_i$ and its gradient on the boundaries. For this end, we subtract Eq. (12) to Eq. (13), to obtain

$$\begin{aligned}\Phi_i(\boldsymbol{x}_0) = &-\int_{S_B} G(r)\boldsymbol{\nabla}(\boldsymbol{\Phi}-\boldsymbol{\Phi}_i)\cdot\boldsymbol{n}dS + \int_{S_B}(\Phi-\Phi_i)\boldsymbol{\nabla}\boldsymbol{G}(r)\cdot\boldsymbol{n}dS -\\ &-\int_{S_W} G(r)\boldsymbol{\nabla}(\boldsymbol{\Phi}-\boldsymbol{\Phi}_i)\cdot\boldsymbol{n}dS + \int_{S_W}(\Phi-\Phi_i)\boldsymbol{\nabla}\boldsymbol{G}(r)\cdot\boldsymbol{n}dS -\\ &-\int_{S_\infty} G(r)\boldsymbol{\nabla}\boldsymbol{\Phi}\cdot\boldsymbol{n}dS + \int_{S_\infty}\Phi\boldsymbol{\nabla}\boldsymbol{G}(r)\cdot\boldsymbol{n}dS\end{aligned} \tag{14}$$

The contribution of the S_∞ integral in Eq. (11) is defined as the undisturbed potential $\varphi^\infty(\mathrm{x}_0)$, namely

$$\varphi^\infty(\boldsymbol{x}_0) = -\int_{S_\infty} G(r)\boldsymbol{\nabla}\boldsymbol{\Phi}\cdot\boldsymbol{n}dS + \int_{S_\infty}\Phi\boldsymbol{\nabla}\boldsymbol{G}(r)\cdot\boldsymbol{n}dS \tag{15}$$

The wake is assumed such that the normal velocity is continuous so that $\partial\Phi/\partial n - \partial\Phi_i/\partial n = 0$. Also, the wake is considered sufficiently thin so that if the thickness of the wake tend to zero

($\delta_W \to 0$), yields

$$\lim_{\delta_W \to 0} \left(- \int_{S_W} G(r)(\partial\Phi/\partial n - \partial\Phi_i/\partial n) dS + \int_{S_W} (\Phi - \Phi_i) \boldsymbol{\nabla} \boldsymbol{G}(r) \cdot \boldsymbol{n} dS \right) = \int_{S_W} (\Phi_U - \Phi_L) \boldsymbol{\nabla} \boldsymbol{G}(r) \cdot \boldsymbol{n} dS \tag{16}$$

where Φ_U is the corresponding value of the total potential in the upper of the wake and Φ_L is the total potential in the lower of the wake. Thus, Eq. (14) reduces to the boundary integral representation for a three-dimensional potential flow in terms of surface singularities represented by sinks and dipoles [10], namely

$$\Phi_i(\boldsymbol{x}_0) = \varphi^\infty - \int_{S_B} G(r) \frac{\partial}{\partial n}(\Phi - \Phi_i) dS + \int_{S_B} (\Phi - \Phi_i) \nabla \boldsymbol{G}(r) \cdot \boldsymbol{n} dS + \int_{S_W} (\Phi_U - \Phi_L) \nabla \boldsymbol{G}(r) \cdot \boldsymbol{n} dS. \tag{17}$$

Equation (17) determines the value of $\Phi_i(\boldsymbol{x}_0)$ in terms of the jumps $\mu = \Phi - \Phi_i$ called dipole strength and $\sigma = \partial\Phi/\partial n - \partial\Phi_i/\partial n$ called sink strength on the boundaries. Then the problem is solved when the distribution of the sink and dipole is determined. In principle, an infinite number of dipole and sink distributions will give the same external flow field, but different internal flow fields. Turning $\Phi_i = \varphi_i^D + \varphi^\infty$ and for convenience making $\varphi_i^D = 0$ (there is no flow inside the body) Eq. (17) reduces to

$$- \int_{S_B} G(r)(\frac{\partial\Phi}{\partial n} - \frac{\partial\varphi^\infty}{\partial n}) dS + \int_{S_B} \varphi^D \boldsymbol{\nabla} \boldsymbol{G}(r) \cdot \boldsymbol{n} dS + \int_{S_W} (\Phi_U - \Phi_L) \boldsymbol{\nabla} \boldsymbol{G}(r) \cdot \boldsymbol{n} dS = 0 \tag{18}$$

Using the boundary condition specified in Eq. (2) then:

$$\sigma = \frac{\partial\Phi}{\partial n} - \frac{\partial\varphi^\infty}{\partial n} = U_N - \frac{\partial\varphi^\infty}{\partial n} = -\frac{\partial\varphi^\infty}{\partial n} \tag{19}$$

Equation (19) is a Neumann kinematics boundary condition which determines the strength of the sinks on the boundary. Thus the first integral on right hand side of Eq. (18) is solved analytically using the constraint given in Eq. (19).

4 Numerical procedure

The potential boundary integral formulation presented in the previous section was recast in a computer program to solve velocities and pressure distribution around an arbitrary body. The basic problem of the present method is the numerical solution of Eq. (18). This requires an evaluation of the integrals and an approximate representation of the body surface. The method assumes that the body surface can be represented by a large number N of triangular and plane quadrilateral elements, typically $N = 10^2$ *to* 10^3, over each of which the sink density and dipole density are assumed constant. This number of grid elements was sufficient to make accurate and

converging results Then the integral equation is replaced by a set of linear algebraic equation for the value of the dipole density on the elements. A typical size of a grid element was taken as 1/20 of the span. The value of the sink density is determined by the Eq. (19). The wake is represented by an infinite vortex sheet emanated from the trailing edge of the lifting body and the lines of vortex are considered straight. The chord makes with the wake an angle θ that is assumed as an input for the numerical code.

The first and the second integrals in Eq. (18) were solved analytically. The grid elements are plane and a local coordinate system was adopted in the center of the element with coordinate $z = 0$. Thus the integrals were solved in the local coordinate along x and y. The unit vector normal to the surface and the area of the grid element were calculated by cross products of vectors in the plane of the element. For the contribution of a grid element about itself the integrals are solved analytically at this particular limit. That means a singularity subtraction is not needed in the present solution. The third integral in Eq. (18) represents the contribution of the vortex sheet to the flow and the magnitude of the horseshoes vortex is equal to the difference of the dipole intensities of the upper and lower panels at the trailing edge adjacent to the wake. This represents physically the Kutta's condition [7] and holds that the vortex filament cannot end in a fluid (Helmholtz's theorem).

Now we suppose a body surface represented by n grid elements and n_w horseshoes vortex. Then Eq. (18) can be re-written

$$\sum_{k=1}^{n} \mu_k C_{jk} + \sum_{k=1}^{n_W} \mu_{wk} C_{jk} = -\sum_{k=1}^{n} \sigma_k B_{jk} \quad j = 1, n \tag{20}$$

where $B_{jk} = \int_{S_k} G_{jk} dS_k$ and $C_{jk} = \int_{S_k} G_{jk} \frac{(\boldsymbol{x}_j - \boldsymbol{x}_k)\cdot \boldsymbol{n}_k}{|\boldsymbol{x}_j - \boldsymbol{x}_k|^2} dS_k$.

Here, C_{jk} is the potential propagator Green's function of the disturbance at the *jth* control point corresponding to a constant μ_k dipole distribution on grid element k and also associated with potential disturbance of a horseshoe vortex with magnitude μ_{wk}, whereas B_{jk} is the potential propagator Green's function of the potential disturbance at the *jth* control point due to a constant σ_k sink distribution on panel k. The values of σ_k are known by Eq. (19) and the values of μ_k and μ_{wk} are found by solving the linear system (20) using a Gauss-Seidel iterative scheme.

To evaluate the velocities and pressures the method of the potential boundary integral has an advantage that the computation of the surface velocity components and pressures is determinable by the local properties of the disturbance potential and by the properties of the undisturbed flow. A local second order distribution is then assumed using dipole values located at five panel centers (a central panel and its four immediate neighbors). The local tangential velocity is then obtained by direct differentiation and the pressure is found using the Bernoulli theorem. The lift coefficient is determined by integration of the surface pressure distribution. The induced drag coefficient is solved by using the integral formulation of the momentum equation in a control volume that ends far downstream of the body (the well known Treffz plane), since the

integration of the pressure cannot result in accurate values of the induced drag coefficient if the grid is coarse [2]. Applying the momentum equation [5] and assuming steady flow and the wake trail from the trailing edge in the direction of the free-stream yields

$$D_i = \frac{\rho}{2} \int_{wake} (\Phi_U - \Phi_L) \frac{\partial \Phi}{\partial n} dl \tag{21}$$

where $\partial\Phi/\partial n$ is the velocity normal to the wake in the treffz plane and l is the length in the spanwise direction. To solve the above equation, we consider control points in the middle of the infinity vortex filaments with intensities $\Phi_U - \Phi_L$ and calculate the velocities induced by the filaments (wake).

5 Application of the method

In order to verify the accuracy of the numerical method, results of our code were compared with analytical, experimental and numerical results based on different methods. Figure 2 compares the analytic potential solution for the flow around a sphere with the numerical solution. The plot shows that the pressure distributions from the computer simulation are in very good agreement with the analytical prediction, $cp = 1 - (9/4)sin^2\theta$, with a maximum error less than 5%.

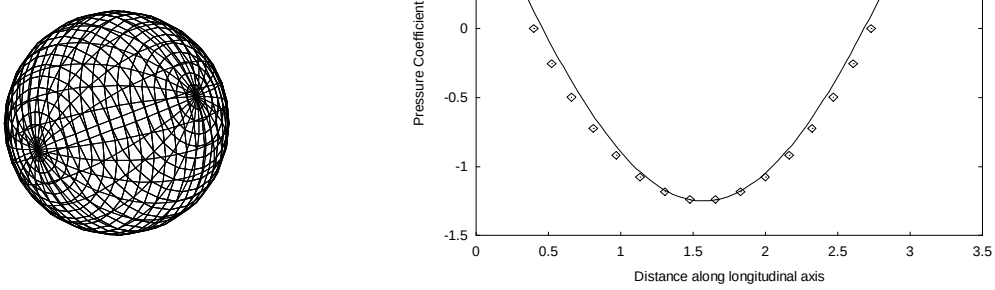

Figure 2: Pressure coefficient around a sphere with radius of $\pi/2$. The diamonds represent the numerical simulation with 800 grid elements and the continuous line represents the potential analytical solution $cp = 1 - (9/4)\sin^2\theta$

In addition, we apply our boundary integral scheme to solve the potential flow around the hemisphere nose shown in Fig. 3. The results of the pressure coefficient corresponding to this axisymmetric potential flow were compared with experimental observation carried out by Cole, 1951. We reproduce the results in our simulation accurate to 5%.

Another application of the potential boundary integral method explored here was the calculation of the pressure distribution around a wing with an aspect ratio of 3 and a taper ratio

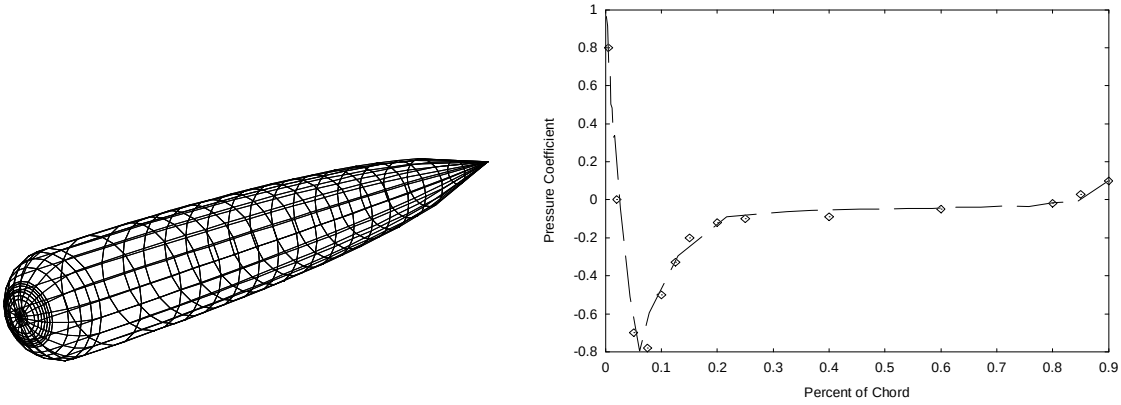

Figure 3: Pressure coefficient along of the longitudinal axis of a body with hemispherical nose. The dashed line represents the numerical simulation with 860 grid elements and the diamonds represent the experimental measurements carried out by Cole, 1952 for Reynolds number 9 x 10^5 based on the body length.

of 0.5. The results are again compared with experimental data of Kolbe and Boltz, 1951 for a Reynolds number of 4 x 10^6 based on the chord length. From the view of the three-dimensional simulated wing shown in Fig. 4, we can see the presence of the leading edge swept back 48.5 $^\circ$, no twist and the sections are the NACA 64A10 in planes inclined 45 $^\circ$ to the plane of the symmetry. Figure 4 shows a comparison between experimental and numerical pressure coefficients in a section of 55% of the semi-span for angles of attack of 6 $^\circ$ and 12 $^\circ$. This plot shows a very good agreement with the experimental results except near the leading edge in the lower surface at high angles of attack where the maximum error is found to be close to 30%. The discrepancy possibly occurs in this location because it is a highly swept wing and the code does not account the leading edge vortex generated in such configuration. It should be important to note that this is not a limitation of the method and we have made recent progress for incorporating the leading edge vortex in the present boundary integral code. Another possibility for the discrepancy is the presence of the boundary layer that is not account in the code. For a highly swept wing, however, the spanwise velocity is considerable and consequently the boundary layer thickness is thick sufficiently at tips to change the pressure at this location.

Figure 5 shows, for the wing shown in Fig. 4, the experimental measurements of the lift coefficient and total drag coefficient for several angles of attack. Predictions of the boundary integral method for the lift coefficient and for the induced drag coefficient (a contribution of the total drag coefficient) were compared with experimental results and with the numerical results of the vortex-lattice method developed by the authors [1]. In order to simulate a wing with symmetric airfoil (NACA 64A10) by using the vortex-lattice method we consider the vortex filaments (bound and trailing vortex) in a plane, i.e., with camber equal zero. We can see that for angles of attack below 15 $^\circ$, the predictions of the boundary integral method agree very well

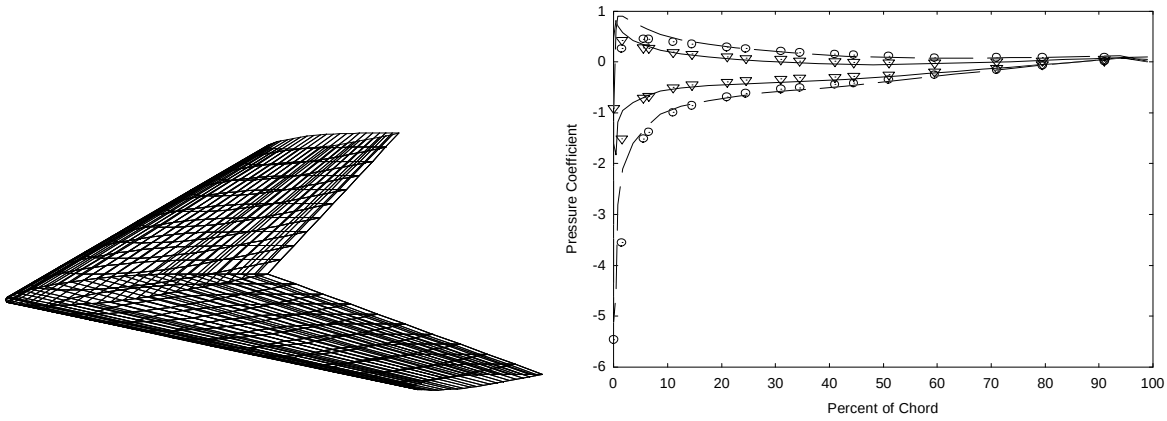

Figure 4: Pressure coefficient around a swept wing at 55% of the semi-span. The continuous line and dashed line represent the numerical simulation with 1000 grid elements for angles of attack of 6 ° and 12 ° respectively. The triangles and circles represent the experimental results for angles of attack of 6 ° and 12 ° respectively and a Reynolds number of 4 x 10^6 based on the chord length.

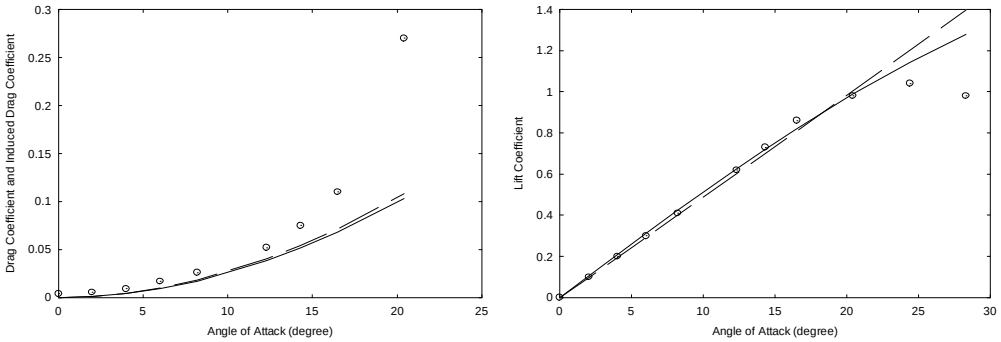

Figure 5: Lift coefficient, drag coefficient and induced drag coefficient for a swept wing. The continuous line represents the predictions of the boundary integral method with 1000 grid elements, the dashed line represents the predictions of the vortex-lattice method with 406 grid elements and the circles represent the experimental measurements with Reynolds number 4x10^6. In the asymptotic limit of small angle of attack (α) the lift coefficient is fitted by the straight line $(1/20)\alpha$.

with the experimental measurements and with the predictions of the vortex-lattice method. For small angle of attack ($\alpha \sim 5^o$) the lift coefficient C_L is fitted by the straight line $C_L = (1/20)$ α. The small scattering observed between experimental and numerical predictions (typically 20%) in the plot of drag coefficient even at small angle of attack is a direct consequence of the viscous drag on the total drag measured experimentally. It should be important to note that the coefficient (1/20) is approximately two times smaller than the corresponding one for

two-dimensional potential flow around a slender airfoil, i.e. $C_L = (\pi^2/90)\ \alpha$.

Above 20 ° of angle of attack, the inaccuracy is due to the separation of the boundary layer that is not account by the method. The induced drag prediction by the boundary integral method is in agreement with the vortex-lattice method.

Figure 6 shows a picture of wind-tunnel in the Fluid Mechanics Laboratory at University of Brasília. The tunnel is subsonic constant total pressure for low to moderate Reynolds number (typically an order of 10^5). The test section is a square of size 460mm. A test was conducted in this wind-tunnel to measure the lift and drag forces of a rectangular wing with aspect ratio of 4. The wing also has a NACA 0012 section and it does not have twist.

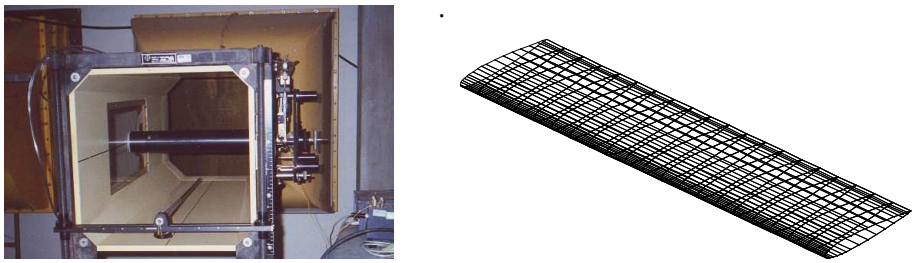

(a) (b)

Figure 6: Experimental setup. (a) wind-tunnel at University of Brasília and (b) wing (NACA0012) simulated and tested.

For the geometry of wing shown in Fig. 6(b), the plots in Figure 7 present experimental measurements of the lift coefficient and total drag coefficient for several angles of attack. The Reynolds number used in theses experiments was 1.6 x 10^5. Predictions of the boundary integral method for the lift coefficient and induced drag coefficient were compared with experimental observations carried out by us and with numerical results based on a vortex-lattice method and also with the classical lifting-line theory which gives the lift and induced drag coefficients in terms of Fourier series [1]. In order to simulate a wing with airfoil NACA 0012 in the Prandtl's lifting-line theory we consider two-dimensional data (i.e. $dCl/d\alpha$ and α for $Cl = 0$) provided by a 2-D panel method implemented by Alvarenga and Cunha [1]. Again, it is seen for angles of attack below 12 ° that the boundary integral method reproduces in very good agreement the mentioned results. However for angle of attack beyond 12 ° the method fails, because the separation of the boundary layer has not been accounted by the theory. In addition, the plot in Fig. 7 show that the induced drag prediction by the boundary integral method is in very good agreement with vortex-lattice method and with lifting-line theory. The observed discrepancy between experimental and numerical results for the drag coefficient is about 25% for an angle of attack of 8^o. This difference is fully attributed to the viscous contribution of the drag that it is not considered in our numerical calculation. Whether however we subtracted from the total drag coefficient given in the experiments the viscous contribution we found an error less that

5%. Finally we see that for small angle of attack the lift coefficient is fitted by the straight line C_L=(13/200) α, that predicts values of C_L about two times smaller than two-dimensional theory.

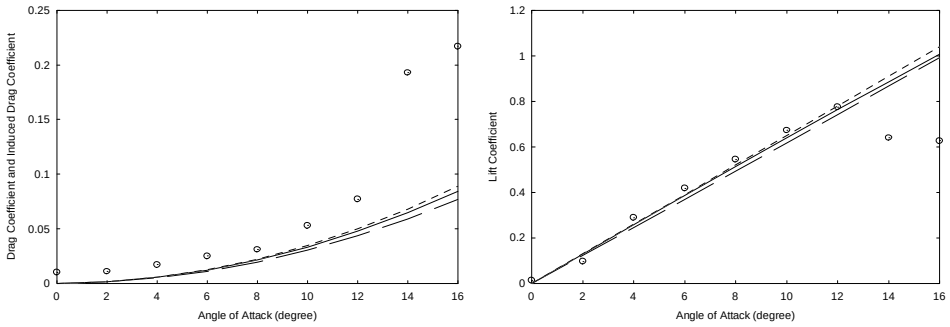

Figure 7: Forces coefficients for an unswept wing. The continuous line represents the predictions of the boundary integral method with 816 grid elements, the dashed line represents the predictions of the vortex-lattice method with 336 grid elements, the dotted line represents the predictions of the lifting-line theory with 60 stations along the span and the circles represent the experimental measurements. The Reynolds number of the experiments was 1.6 x 10^5.

6 Conclusions

In this paper we have presented numerical results for three-dimensional potential flow by using a boundary integral scheme. The simplicity of piecewise constant singularity grid elements offer great flexibility for application to arbitrary bodies. Time is saving to calculate the on-body velocities compared with another boundary integral formulations. The numerical scheme capture the basic aspect of three-dimensional potential flows and create possibilities to study the local aerodynamic characteristics of the flow. The lifting-line theory and vortex-lattice method cannot provide details of the flow as rich as the boundary integral method. The low computing cost and high accuracy makes it practical to apply the present method to problems requiring iterative solutions, e.g., wake-relaxation for high-lift bodies, viscous-inviscid coupled boundary layer calculations, time-stepping calculations for unsteady flows, iterative schemes for transonic flows and optimization routines for design codes. All results given in our code were in very good agreement with the experiments. So we are encouraged to look further.

Acknowledgements. The authors acknowledges the financial support from CAPES, CNPq and FINATEC-UnB. The authors wish to thank prof. Aldo João de Sousa and prof. Jorge Almeida Ferreira for help in the experimental part.

References

[1] R. C. Alvarenga and F. R. Cunha. High Reynolds number flows with applications in aerodynamics. Internal, University of Brasilia – Mechanical Engineering Department, 2004. p.209.

[2] D. L. Ashby. Potential flow theory and operation guide for the panel code pmarc_14. Technical report, NASA TM-1999-209582, 1999. p.45.

[3] D. L. Ashby, M. R. Dudley, and S. K. Iguchi. Development and validation of an advanced low-order panel method. Technical report, NASA TM-101024, 1988.

[4] F. R. Cunha, A. J. Sousa, and M. Loewenberg. A mathematical formulation of the boundary integral equations for a compressible stokes flow. *Computational and Applied Mathematics*, 22:53–73, 2003.

[5] I. Droo and S. Smith. The computation of induced drag with nonplanar and deformed wakes. *SAE PAPER*, 901933:1880–1888, 1990.

[6] J. L. Hess. Calculation of potential flow about arbitrary three-dimensional lifting bodies. Technical Report MDC J5679-01, Douglas Aircraft Company – McDonnell Douglas Corporation, 1972. p.160.

[7] J. L. Hess. The problem of three-dimensional lifting potential flow and its solution by means of surface singularity distribution. *Computer Methods in Applied Mechanics and Engineering*, 4:283–319, 1974.

[8] J. L. Hess. Panel methods in computational fluid dynamics. *Annual Review of Fluid Mechanics*, 22:255–274, 1990.

[9] J. L. Hess and A. M. O. Smith. Calculation of potencial flow about arbitrary bodies. *Progress in Aeronautical Sciences*, 3:138, 1966.

[10] B. Hunt. The panel method for subsonic aerodynamic flows: A survey of mathematical formulations and numerical models and an outline of the new british aerospace scheme. *Von Karman Institute for Fluid Dynamics, Lecture Series 1978-4*, March 13-17 1978.

[11] O. D. Kellogg. *Foundations of Potential Theory.* Dover Publications, Inc., New York, 1954. p.384.

[12] U. Lemma and L. Morino. Transonic two dimensional analysis using a boundary integral equation method. *Journal of Fluids and Structures*, 11(4):247–269, 1997.

[13] L.Gebharedt, D. Fokin, T. Lutz, and S. Wagner. An implicit-explicit dirichlet-based field panel method for transonic aircraft design. *AIAA-2002-3145*, page 13, 2002.

[14] M. J. Lighthill. *An Introduction to Fourier Analysis and Generalised Functions.* CUP, Cambridge, 5th edition, 1980. p.79.

[15] B. Maskew. Prediction of subsonic aerodynamic characteristics: A case for low-order panel methods. *Journal of Aircraft*, 19(2):157–163, 1982.

[16] B. Maskew and F. A. Woodward. Symmetrical singularity model for lifting potential flow analysis. *Journal of Aircraft*, 13(9):733–734, 1976.

[17] L. Morino, L. T. Chen, and E. O. Suciu. Steady and oscillatory subsonic and supersonic aerodynamics around complex configurations. *AIAA Journal*, 13(3):368–374, 1975.

[18] L. Morino and C. C. Kuo. Subsonic potential aerodynamics for complex configurations: A general theory. *AIAA Journal*, 12(2):191–197, 1974.

[19] L. Morino and U. Lemma. Boundary integral equations and conservative dissipation schemes for full potential transonic flows. *Computational Mechanics*, 13:90–99, 1993.

[20] O. C. Resende. The evolution of the aerodynamic design tools and transport aircraft wings at embraer. *Journal of the Brazilian Society of Mechanical Science & Engineering*, 26(4):379–390, 2004.

[21] J. E. Romate. Local error analysis of three-dimensional panel methods in terms of curvilinear surface coordinates. *SIAM Journal of Numerical Analysis*, 27(2):529–542, 1990.

[22] P. E. Rubbert and g. R. Saaris. A general three-dimensional potential-flow method applied to V/STOL aerodynamics. *SAE Paper*, 680304:945–957, 1968.

[23] N. Singh, G. Bandyopadhyay, and B. C. Basu. Calculation of potential flow about arbitrary three dimensional wings using internal singularity distributions. *Aeronautical Quarterly Journal*, pages 197–211, 1983.

[24] E. N. Tinoco, D. N. Ball, and F. A. Rice. PAN AIR analysis of a transport high-lift configuration. *Journal of Aircraft*, 24(3):181–187, 1987.

[25] F. A. Woodward. Analysis and design of wing-body combinations at subsonic and supersonic speeds. *Journal of Aircraft*, 5(6):528–533, 1968.

[26] F. A. Woodward and E. J. Landrum. The supersonic triplet - a new aerodynamic panel singularity with directional properties. *AIAA Journal*, 18(2):138–142, 1980.